Appl Microbiol Biotechnol (2017) 101:2801–2809
DOI 10.1007/s00253-017-8099-6

Nanostructured ZnO films on stainless steel are highly safe and effective for antimicrobial applications

Kyudae Shim[1,2] · **Mohamed Abdellatif**[2] · **Eunsoo Choi**[1] · **Dongkyun Kim**[1]

Received: 28 October 2016 / Revised: 20 December 2016 / Accepted: 27 December 2016 / Published online: 7 January 2017

Abstract The safety and effectiveness of antimicrobial ZnO films must be established for general applications. In this study, the antimicrobial activity, skin irritation, elution behavior, and mechanical properties of nanostructured ZnO films on stainless steel were evaluated. ZnO nanoparticle (NP) and ZnO nanowall (NW) structures were prepared with different surface roughnesses, wettability, and concentrations using an RF magnetron sputtering system. The thicknesses of ZnO NP and ZnO NW were approximately 300 and 620 nm, respectively, and ZnO NW had two diffraction directions of [0002] and [01–10] based on high-resolution transmission electron microscopy. The ZnO NW structure demonstrated 99.9% antimicrobial inhibition against *Escherichia coli*, *Staphylococcus aureus*, and *Penicillium funiculosum*, and no skin irritation was detected using experimental rabbits. Approximately 27.2 ± 3.0 μg L^{-1} Zn ions were eluted from the ZnO NW film at 100 °C for 24 h, which satisfies the WHO guidelines for drinking water quality. Furthermore, the Vickers hardness and fracture toughness of ZnO NW films on stainless steel were enhanced by 11 and 14% compared to those of the parent stainless steel. Based on these results, ZnO NW films on STS316L sheets are useful for household supplies, such as water pipes, faucets, and stainless steel containers.

Keywords Zinc oxide nanostructure · Antimicrobial activity · Skin irritation · Elution behavior · Mechanical properties

Introduction

As public health standards have improved, interest in the quality of drinking water has greatly increased (Dietrich and Burlingame 2015). Furthermore, over time, the necessity for hygienic conditions in the household environment has increased (Byarugaba 2004; Cao et al. 2010). The propagation of harmful bacteria and fungi depends on environmental factors, such as humidity and temperature. In particular, a rise in humidity caused by the presence of water or other fluids favors an increase in the number of microbes (Makris et al. 2014). Therefore, despite an interest in maintaining sanitary lifestyles, microbes in water pipes, faucets, and containers made of stainless steel can cause tap water pollution and have become a serious problem (Okeke et al. 2005). In particular, there are various bacteria such as gram-negative (*Escherichia coli* and *Vibrio cholerae*) and gram-positive (*Bacillus cereus* and *Staphylococcus aureus*) bacteria in polluted water, and these bacteria can cause food poisoning (Josephs-Spaulding et al. 2016; Vasudevan and Oturan 2014). In addition, fungi (*Penicillium funiculosum*) having spores are also found in many households, and they cause rhinitis and asthma (Djemai-Zoghlache et al. 2011). To remove harmful microbes, the washing of stainless steel products with alcohol or alkaline solutions has been encouraged. However, these methods cannot maintain long-lasting antibiosis activity (Martin et al. 2016). Therefore, research has actively focused

Electronic supplementary material The online version of this article (doi:10.1007/s00253-017-8099-6) contains supplementary material, which is available to authorized users.

✉ Dongkyun Kim
kim.dongkyun@hongik.ac.kr

[1] Department of Civil Engineering, Hongik University, 94 Wausan-ro, Mapo-gu, Seoul 04066, Republic of Korea

[2] GS Engineering and Construction, Gran Seoul, 33 Jong-ro, Jongno-gu, Seoul 03159, Republic of Korea

on potent antibacterial films that use metal ions on stainless steel substrates (Sin et al. 2014).

Generally, silver, copper, and zinc ions are popular antimicrobial agents (Boveris et al. 2012; He et al. 2011; Gholap et al. 2016); silver ions are particularly powerful. The minimum bactericidal concentration (MBC) of metal ions for zinc oxide (ZnO) films is greater than 5000 μg mL^{-1} against various microbes (Ren et al. 2009). The MBC value for silver oxide is only 100 μg mL^{-1} (Ren et al. 2009). However, chromodermatosis develops when the skin is exposed to silver ions (Parikh et al. 2005; Kumar and Münstedt 2005). There are also reports of the toxicity of silver nanoparticles and compounds owing to accumulation in the body (Djeribi et al. 2012; Drake and Hazelwood 2005). Therefore, many recent studies have investigated zinc ions, instead of silver ions, as antimicrobial agents and coating materials (Kuang et al. 2016; Madhumitha et al. 2016).

Although zinc ions are effective antimicrobial agents, they exhibit below-average antimicrobial activity. To increase the antimicrobial activity of ZnO films, it is necessary to increase the contact area between zinc ions and microbes by nanostructuring. Recently, various ZnO nanostructures, nanowires, nanorods, nanotubes, nanobelts, nanoparticles (NPs), and nanowalls (NWs) have been fabricated using a radio-frequency (RF) magnetron sputtering system because surface area is an important factor for reactivity (Choi et al. 2015; Tamvakos et al. 2015). ZnO NWs have broad applications owing to their larger surface area than those of other ZnO nanostructures (Saravanakumar and Kim 2014). In addition, the RF magnetron sputtering system enables precise control of film thickness under high-vacuum conditions and to fabricate homogeneous densified films (Tamvakos et al. 2015). Therefore, prevention of delamination between antimicrobial films and stainless steel substrates is useful and is expected to improve durability.

The antimicrobial activity of ZnO thin films is well established, but few studies have examined the skin irritation and mechanical properties of various ZnO nanostructures. Furthermore, toxicity standards have been established by the World Health Organization (WHO), which requires an elution limit of 3000 μg L^{-1} zinc ions (Ashworth and Alloway 2004). However, few studies have evaluated zinc ion elution using ZnO films. The purpose of this study was to evaluate the antimicrobial activity of nanostructured ZnO films against *E. coli*, *S. aureus*, and *P. funiculosum*. In addition, the skin irritation, elution behavior, and mechanical properties (Vickers hardness and fracture toughness) of ZnO thin films on stainless steel (STS316L) were measured to determine whether this material could be used in household supplies, such as water pipes, faucets, and stainless steel containers.

Materials and methods

Preparation of nanostructured ZnO films

ZnO films were fabricated on STS316L substrates using the RF magnetron sputtering system (SNTek, Suwon, Korea). The STS316L substrates were polished with SiC paper and diamond suspensions for microstructure observations and ZnO film deposition, ultrasonicated, treated with ethanol and deionized water for 5 min each, and blown dry with high-purity N_2 gas. The chamber was evacuated to below 3.0×10^{-3} mTorr, with working pressure during deposition fixed at 2.5 mTorr. The ratio of the partial pressure of $Ar:O_2$ was kept at 17:3. The substrate holder was rotated at 20 rpm to obtain a film with a uniform thickness and uniform composition. Then, the ZnO films (NPs and NWs) were fabricated with various deposition times from 20 to 40 min at 280 °C using an RF power of 130 W at the Zn target (Kojundo, Sakado, Japan) of 99.99% purity.

Characterizations of ZnO films

Field emission scanning electron microscopy (FESEM; JSM-7001F, Tokyo, Japan) enabled the determination of surface morphology and thickness of ZnO films. The energy dispersive X-ray spectroscopy (EDS; Inca Energy 250, High Wycombe, UK) profile of the ZnO film served to estimate the concentration of Zn. The average surface roughness (R_a) values of the ZnO films were estimated by atomic force microscopy (AFM; Veeco Instruments, Plainview, NY, USA) in a scanned area of 500 × 500 nm^2. The water contact angles (CA) were measured at room temperature using a drop shape analyzer (DSA 100/Krüss, Hamburg, Germany) with water droplets of approximately 3.0 μL. The crystalline phase was determined by X-ray diffraction (XRD; D/MAX-2500H, Tokyo, Japan) with Ni-filtered Cu Kα radiation (λ = 1.54 Å) in the range of $30° \leq 2\theta \leq 50°$ at a scan rate of 4° min^{-1}. The crystalline size (L) and full-width at half maximum value of the ZnO film were calculated using the Scherrer equation (Žvab et al. 2012). XRD patterns served to calculate the interplanar (d) spacing using Bragg's law (Kumar et al. 2014). High-resolution transmission electron microscopy (TEM; JEM-2100F, Tokyo, Japan) allowed the determination of nanostructure and lattice distance of ZnO films, as well as confirming intracellular and morphological alterations in microbial cells on treated ZnO films.

Microbial strains and cultivation

Standard strains of bacteria, i.e., *E. coli* (ATCC 8739) and *S. aureus* (ATCC 6538), and a standard strain of the fungus *P. funiculosum* (ATCC 11797) were used to evaluate antibacterial and antifungal activity, respectively. The Korean Culture

Center of Microorganisms provided the strains. *E. coli* was cultured in nutrient agar medium (Difco 0001; 1.0 L of distilled water, 3.0 g of beef extract, 5.0 g of peptone, 15.0 g of agar, pH 7.0) for 24 h at 37 °C, *S. aureus* was cultured in trypticase soy agar (BBL 4311768; 1.0 L of distilled water, 17.0 g of pancreatic digest of casein, 3.0 g of pancreatic digest of soybean meal, 5.0 g of NaCl, 2.5 g of K_2HPO_4, 2.5 g of glucose, 15.0 g of agar) for 24 h at 37 °C, and *P. funiculosum* was cultured on potato dextrose agar (BBL 7149; 1.0 L of distilled water, 300.0 g of diced potatoes, 20.0 g of glucose, 15.0 g of agar) for 48 h at 24 °C.

Antimicrobial activity tests

Antibacterial and antifungal activities of ZnO films were evaluated using the second edition of the International Organization for Standardization (ISO) 22196 method. The scope of this method has been extended to include surfaces made of non-porous materials other than plastic, ensuring applicability to various antimicrobial products such as ZnO nanostructured materials. The parent STS316L substrate and the substrate treated with ZnO consisted of 10 mm × 10 mm squares. Before preparing dilutions, all equipment was sterilized in an autoclave at 121 °C for 15 min. Substrates were cleaned by soaking in ethanol (70%) for 5 min and wiped with distilled water. The dilution plating technique enabled all microbes (*E. coli*, *S. aureus*, and *P. funiculosum*) to have concentrations between 2.0×10^5 and 5.0×10^5 colony forming units per milliliter (CFU mL^{-1}). The diluted bacterial suspensions with cell concentrations of about 10^5 CFU mL^{-1} were injected (about 0.1 mL $well^{-1}$) onto the parent STS316L and ZnO films in a 24-well culture plate. A sterilized polyethylene film was adhered to the parent stainless steel substrate and the substrate with ZnO for microbe attachment. After 1 h, 1.0 mL of liquid medium was poured into each well, and 0.1 mL of mixed liquid medium was transferred to solid culture medium. Solid culture medium substrates containing microorganisms were maintained in a biochemical oxygen demand incubator for 24 h: *E. coli* and *S. aureus* at 37 °C, and *P. funiculosum* at 24 °C. After incubation, the number of surviving microbial cells was counted and expressed as log CFU mL^{-1}. All antimicrobial tests were repeated ten times.

Skin irritation and elution tests

The Korea Testing and Research Institute evaluated skin reactions to ZnO NWs in accordance with ISO 10993–5:2009(E), using New Zealand white (NZW) rabbits. The skin of NZW rabbits was shaved, then separated into test and control sites (each of 25 × 25 mm^2) by a partition. The epidermis of test sites was scratched using a needle. ZnO NWs on the STS316L substrate were spread onto the intact and abraded skin. After spreading, the test and control (treated with sterile water) sites on the skin were covered and fixed with pasteurized gauze affixed with tape. Animal weights and survival were confirmed at 24 and 72 h after exposure to the ZnO NWs. The primary irritation index (P.I.I.) was determined by scoring the edema and red spots at 24 and 72 h after ZnO exposure (Mishra et al. 2016). A score of 0 points indicated no edema or red spots and 4 points indicated a wound longer than 1.0 mm. The material was classified as a non-irritant ($0 \leq$ P.I.I. ≤ 0.5), mild irritant ($0.6 \leq$ P.I.I. ≤ 2.0), moderate irritant ($2.1 \leq$ P.I.I. ≤ 5.0), or severe irritant ($5.1 \leq$ P.I.I. ≤ 8.0). The P.I.I. values of films with ZnO were confirmed using six NZW rabbits. Inductively coupled plasma atomic emission spectroscopy (ICP-AES; Optima-4300 DV/Perkin-Elmer, Shelton, USA) enabled the evaluation of Zn ions elution from ZnO films and thus the determination of whether the material met the WHO threshold of 3000 μg L^{-1} (Ashworth and Alloway 2004). The ZnO film on the STS316L substrate (10 mm × 10 mm^2) was placed in drinking water (100 mL) and the concentration of eluted Zn ions was confirmed after various times ranging from 1 to 24 h in a water bath at 100 °C.

Mechanical property tests

A Vickers micro-hardness tester (MXD-CX3E, Kobe, Japan) with a 4.91 N load and a loading time of 30 s allowed the measurement of the ZnO films durability on the STS316L substrate. Vickers hardness (H_V) was determined based on the indentation size using the ASTM C 1327-08 standard method. The fracture toughness (K_{IC}) was calculated based on the propagated crack length from the indentation according to ASTM E 1820–11.

Results

Characterizations of the ZnO thin films

To evaluate the antimicrobial activity of nanostructured ZnO films on stainless steel substrates, ZnO NP and NW films with different surface morphologies were deposited by RF magnetron sputtering with deposition times of 20 and 40 min, as shown in Fig. 1. The surface morphology of the ZnO NW structure was similar to those of entangled nanoparticles and nanowires. The thickness was approximately 620 nm, and the widths of the newly formed NWs were approximately 42 nm. Using a deposition time of 20 min, the thickness of ZnO NPs was approximately 300 nm, and the NPs showed a smoother surface than the ZnO NW. The differences in surface morphology are attributable to inhibition of the synthesis of the nanowall network at the surface of the different substrates. Therefore, reduction of deposition time (initial deposition of a film on the stainless steel substrate) can decrease the

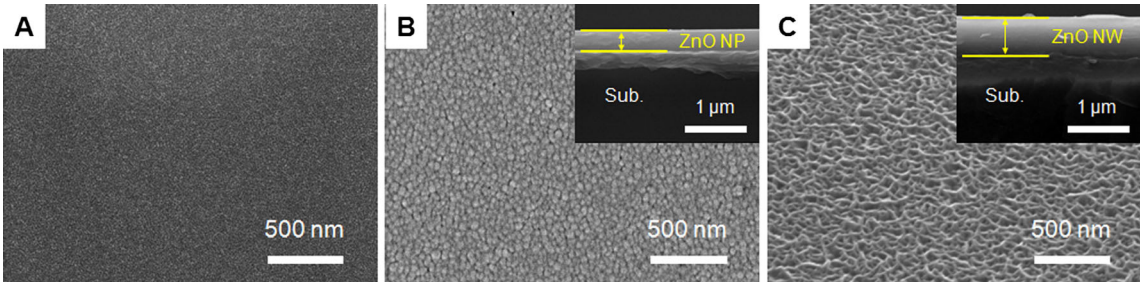

Fig. 1 Top-view field emission scanning electron microscopy images of ZnO thin films. **a** Parent STS316L. **b** ZnO NP. **c** ZnO NW. The *insets* show cross-sectional views demonstrating the thickness of the ZnO films on the STS316L substrates

activation energy of nucleation for sufficient nanostructure synthesis.

Figure S1 shows the XRD peaks of the ZnO films prepared using different structures. The detailed crystalline structures from the XRD analysis are indicated in Table 1. As shown in Fig. S1, a (002) plane in a well-ordered hexagonal structure typical of ZnO crystalline structures was observed (Jain et al. 2013). This was attributed to the low surface energy required for the formation of the (002) plane in the *c*-direction. In comparison, the crystallinity of ZnO NW was higher than that of ZnO NP, as indicated by higher diffraction peak intensity, whereas the full-width at half maximum value was lower (0.23° for NPs; 0.21° for NWs). For the ZnO NW structure, a new diffraction peak of the (100) plane appeared at 31.1°. The formation of a new diffraction plane in the ZnO NW structure associated with an increase in the *d*-spacing. An increase in crystal size owing to the higher crystallinity of ZnO NW and the formation of the (100) plane changed the cell volume and lattice parameter, resulting in a uniform compressive strain (Acocella et al. 2016). The prominent diffraction peaks of ZnO shifted ($\Delta 2\theta = 0.2°$) from 34.6° for NP to 34.4° for NW.

As shown in Fig. S2, the crystallinity of the ZnO NW was confirmed by high-resolution TEM. Figure S2a shows cross-sectional images of the ZnO NW film prepared using a deposition time of 40 min. The ZnO NW film consisted of a vertical ZnO NP (Fig. S2b) region until the thickness reached approximately 300 nm and a ZnO NW (Fig. S2c) region. The ZnO NW region had two diffraction directions of [0002] and [01–10], consistent with the results of the XRD analysis. Under thermodynamic equilibrium, facets with a high surface energy generally have a small area, whereas facets with a relatively lower surface energy are larger (Choi et al. 2015; Saravanakumar and Kim 2014). Different structures of ZnO films could induce differences in the anisotropic growth direction. Clearly, when examining the growth of the ZnO film, the highest growth rate was along the [0002] direction of the *c*-axis and the largest facet was generally in the [01–10] direction. Growth in this direction can form the NW structure; therefore, our results confirm that by controlling the growth conditions, it is possible to change the surface structure of ZnO films.

Table 1 XRD results for the ZnO NP and ZnO NW generated with various deposition times

Samples	Diffraction plane (hkl)	2θ (°)	*d*-spacing (nm)	FWHM (°)	Crystalline size (nm)
STS316L	(110)	44.7	0.202	0.24	36.5
ZnO NP	(002)	34.6	0.258	0.23	36.2
ZnO NW	(002)	34.4	0.260	0.21	39.0

Figure 2 shows the surface roughness and wettability of the parent STS316L substrate, ZnO NP, and ZnO NW. The antimicrobial effect depends on interactions between Zn ions and microbes on the substrate surface (Madhumitha et al. 2016). Therefore, we expected the patterned nanostructures, such as ZnO NWs, to lead to high levels microbe attachment and proliferation owing to their high surface energy, high surface roughness, and improved wettability. The surface roughness of the ZnO NW film was higher than that of the parent stainless steel (from 1.3 to 6.4 nm). As shown in Table 2, the water contact angle of the NW structure was lower (i.e., 85° for parent stainless steel vs. 71° for the ZnO NW film). The nanostructured ZnO film had a higher antimicrobial effect as the concentration of Zn ions increased on the substrate surface. Based on the EDS analysis summarized in Fig. 1b, c, the surface concentration of Zn ions for the ZnO NP and NW films ranged from 24.3 to 31.7 wt.%. Therefore, based on an evaluation of the antimicrobial activity of nanostructured ZnO films, an increase in the Zn ion concentration on the surface increased the surface roughness, thereby increasing the contact region between the microbes and Zn ions.

Antimicrobial activity

Figure S3 shows the numbers of colonies for three microbial strains (*E. coli*, *S. aureus*, and *P. funiculosum*) on the plates. The parent STS316L substrate did not prevent the growth of *E. coli* (4.598 ± 0.103 log CFU mL^{-1}), *S. aureus*

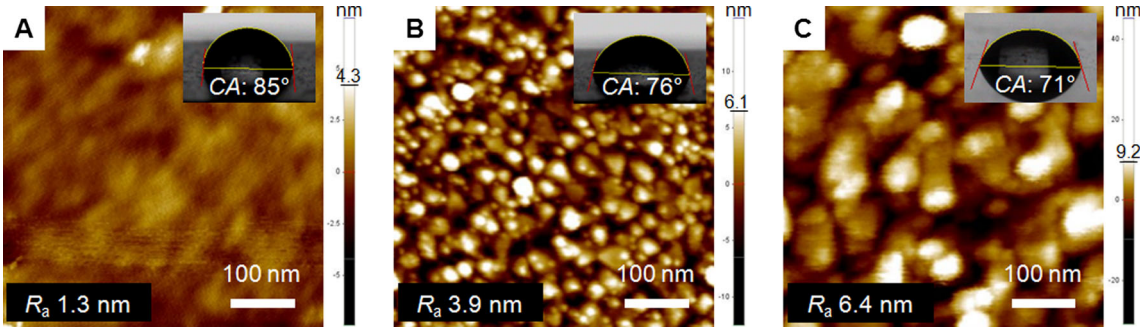

Fig. 2 Atomic force microscopy images of ZnO thin films. **a** Parent STS316L. **b** ZnO NPs. **c** ZnO NWs. The *insets* show the water contact angle of droplets on the parent substrate and ZnO films

(5.015 ± 0.135 log CFU mL^{-1}), and *P. funiculosum* (5.315 ± 0.112 log CFU mL^{-1}). The ZnO NP-supplemented films exhibited antimicrobial activity (<1.4 log CFU mL^{-1}). In particular, the ZnO NW structure, which had a high surface roughness, a high Zn concentration on the surface, and low contact angle, exhibited few colonies, achieving antibacterial inhibition of greater than 99.9%. The numbers of colonies for the ZnO NW structure were as follows: *E. coli* (0.498 ± 0.084 log CFU mL^{-1}), *S. aureus* (0.594 ± 0.071 log CFU mL^{-1}), and *P. funiculosum* (0.618 ± 0.093 log CFU mL^{-1}). Therefore, the antimicrobial activity of the nanostructured ZnO films was substantially higher than that of the parent substrate. These results confirmed that the ZnO NW structure increased the contact area between microbes and Zn ions.

Morphological analysis of microbes

The morphological differences between the microbes on the parent substrate and ZnO NW film were examined by FESEM and TEM. All bacteria and fungi exposed to Zn ions were damaged or had rougher surfaces than those of microbes cultured on the parent stainless steel. Based on these findings and the results obtained for microbial colonies cultured on plates in Fig. 3, ZnO NW could lead to the inactivation of microbes, with high antimicrobial activity. The transmission electron micrographs of bacteria and fungi are shown in Fig. 4. The *S. aureus* (Fig. 4a, c) and *P. funiculosum* (Fig. 4b, d) cells exhibited morphological damage owing to direct reciprocal action between the ZnO NW film and microbial cell surfaces. Previous reports have indicated that metal ions, such as antimicrobial Zn, Ag, and Cu, enter microbial cells, resulting in oxidative stress (Imlay 2013; Jain et al. 2013). Consistent with these previous observations, cell growth and recovery decreased, and the microbes that contacted the ZnO NW film eventually died.

Evaluation of skin irritation and elution behavior

Skin irritation caused by ZnO NW films and the elution concentration were evaluated to demonstrate whether this material was suitable for applications to household supplies, such as door handles, water pipes, faucets, and stainless steel containers. A skin irritation test was conducted in six NZW rabbits. The NZW rabbits have known sensitivity toward the test materials. For the ZnO NW film to be considered safe, the P.I.I. value must be in the non-irritant range ($0 \leq$ P.I.I. ≤ 0.5). As shown in Fig. S4, the P.I.I. value was 0, which is within the non-irritant range. After 24 and 72 h of ZnO NW exposure (Fig. S4b, c), skin irritation indicators, such as inflammation, red spots, and a skin rash, were not detected in either abraded or intact skin regions. In addition, no animals showed mortality or rapid weight changes during the skin irritation experiment. Based on these results, the ZnO NW film was classified as a non-irritant.

The elution behavior of the ZnO NW film is also an important factor for drinking water safety or prolonged use. A Zn^{2+} ion limit in drinking water has been established by WHO guidelines (under 3000 μg L^{-1}). Therefore, it is necessary to determine the concentration of eluted Zn ions for applications to household supplies. As shown in Table 3, the Zn ion concentrations for ZnO NP and NW were 20.9 ± 2.4 and 27.2 ± 3.0 μg L^{-1} at 100 °C after 24 h in the elution test. Therefore, all specimens were within the WHO standard limit of 3000 μg L^{-1}. The enhanced proliferation of the ZnO NW film can be explained by the higher surface energy conferred by nanostructuring. This film exhibited improved wettability and a lower water contact angle, which increase microbe attachment and proliferation (Choi et al. 2015; Tamvakos et al. 2015).

Table 2 Water contact angles of the parent STS316L substrate and the ZnO NP and NW films measured using distilled water

Samples	Contact angle (°)	Wetting energy (mN m^{-1})	Spreading coefficient (mN m^{-1})	Adhesion strength (mN m^{-1})
STS316L	85.3 ± 1.1	5.9	66.8	78.7
ZnO NP	76.2 ± 0.8	16.9	55.9	89.8
ZnO NW	71.4 ± 1.2	23.2	49.6	96.0

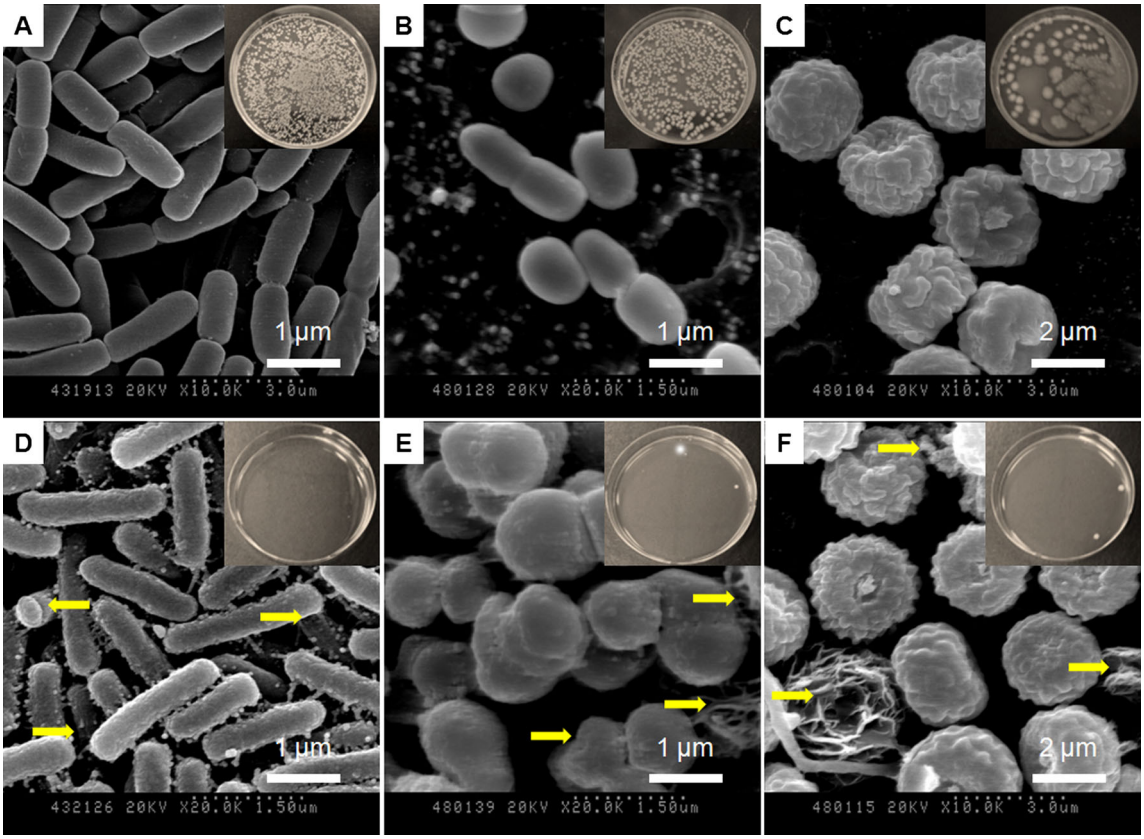

Fig. 3 Field emission scanning electron micrographs of untreated microbes (**a**–**c**), and microbes treated (**d**–**e**) with ZnO NW. **a**, **d** *Escherichia coli*. **b**, **e** *Staphylococcus aureus*. **c**, **f** *Penicillium funiculosum*. The *insets* show images of microbial colonies cultured on each plate

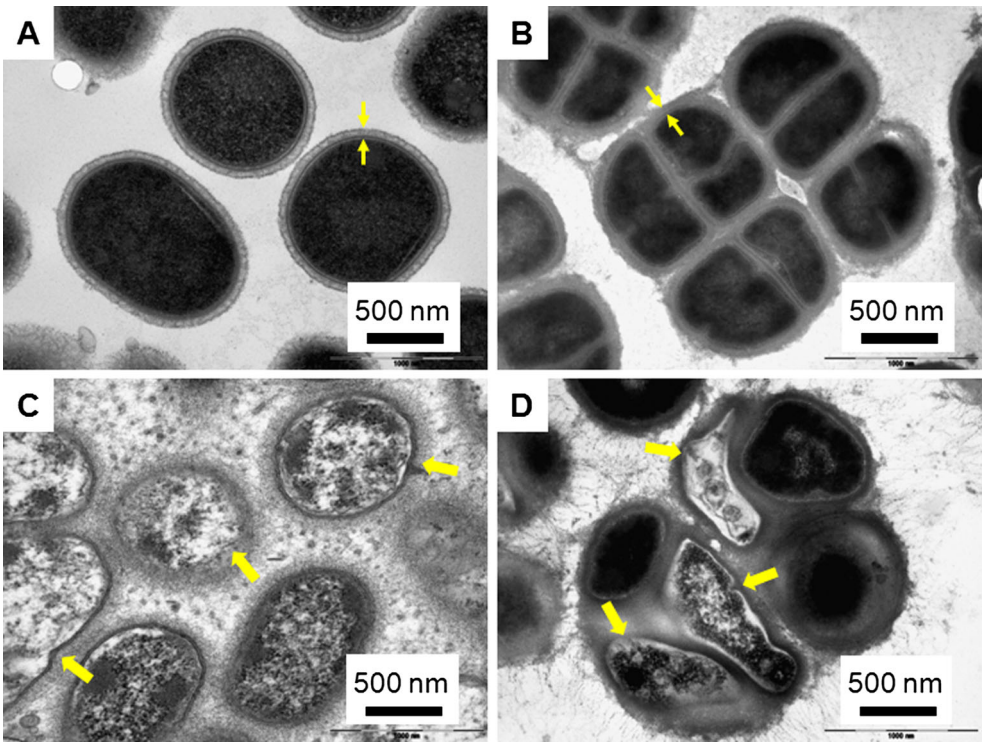

Fig. 4 Transmission electron micrographs. **a**, **b** Parent STS316L, **c**, **d** Treated with ZnO NW. **a**, **c** *Staphylococcus aureus*. **b**, **d** *Penicillium funiculosum*

Table 3 Concentration of eluted Zn ions from ZnO NP and ZnO NW deposited on STS316L at 100 °C determined at various elution times (1–24 h)

Samples	Concentration of eluted Zn ions (μg L^{-1})			
	1 h	6 h	12 h	24 h
ZnO NP	0.8 ± 0.1	6.3 ± 0.5	11.7 ± 1.8	20.9 ± 2.4
ZnO NW	1.2 ± 0.2	8.4 ± 0.6	14.1 ± 1.6	27.2 ± 3.0

Mechanical properties

For ZnO films to be used in household supplies for extended periods, stainless steel substrates with ZnO must be characterized by high H_V and K_{IC}. Figure 5 shows the mechanical properties of ZnO films on STS316L substrates. H_V is defined as the resistance of the concentrated load in a local region, and K_{IC} is the capacity of the ZnO film to contain a crack and resist fracturing (Rouxel et al. 2014; Sellappan et al. 2013). The H_V values at the same load (4.9 N) for substrates with the ZnO films fabricated using ZnO NP and NW were 0.860 ± 0.022 and 0.899 ± 0.021 GPa, respectively. K_{IC} values of ZnO NP and NW films were 0.473 ± 0.027 and 0.518 ± 0.026 MPa·$m^{1/2}$, respectively. The mechanical properties of stainless steel are considerably influenced by their crystalline size, density, and cracking. Generally, metallic materials did not exhibit cracking on the surface before reaching a plastic deformation state; however, cracks could be detected if voids or inclusions are present on the surface (Sellappan et al. 2013). Therefore, surface coating on substrates is a suitable method to provide strength. Additionally, the thickness of thin films is proportional to the mechanical properties (Rouxel et al. 2014). Therefore, as the thickness increased from 300 nm (NPs) to 620 nm (NWs), the H_V and K_{IC} values increased owing to the higher rate of resistance failure of ZnO NW. This H_V and K_{IC} values of ZnO NW were higher than those of parent stainless steel by approximately 11 and 14%, respectively.

Discussion

Owing to their antimicrobial activity, Zn ions are used in water purification and filtration systems, door handles, and household supplies. ZnO films and components are well-known antibacterial agents, but their skin irritation properties and elution behavior have not been extensively examined. Therefore, we examined the antimicrobial activity of ZnO films as a function of their nanostructure (NP and NW), surface Zn concentration, surface roughness, and wettability. We also evaluated their skin irritation properties and elution behavior. In addition, the H_V and K_{IC} values were measured to confirm whether ZnO thin films could be applied broadly to household products.

In a preliminary experiment, the thickness of ZnO films increased from 300 to 620 nm (for the same deposition conditions) when the deposition time was increased from 20 to 40 min, and the structures of the ZnO film also changed from nanoparticles to a combined structure of entangled nanoparticles and nanowires. Generally, deposition conditions, such as the partial pressure of oxygen gas, substrate temperature, and deposition time, are associated with nanostructural changes in ZnO films (Choi et al. 2015; Zhang et al. 2014). ZnO NW

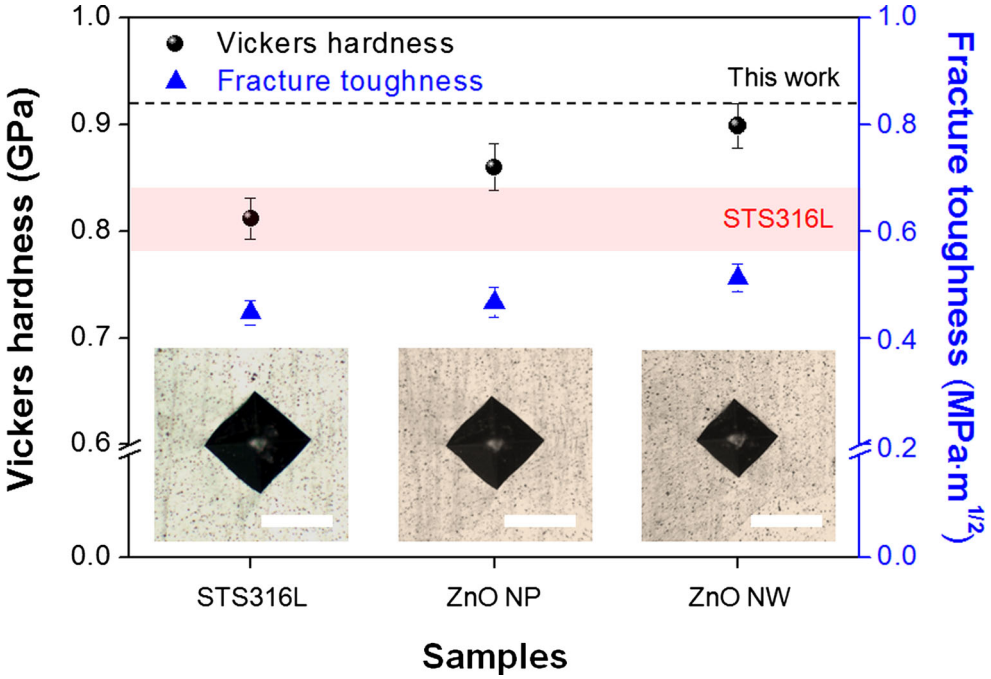

Fig. 5 Vickers hardness and fracture toughness of ZnO films on STS316L substrates: *Inset* shows the micrographs of intensity at 4.9 N load; *scale bar* is 100 μm

formation was attributed to a vapor–solid mechanism (Biroju et al. 2013). In the initial stage, the ZnO thin film of NPs was deposited on the stainless steel substrate. As the thickness of the ZnO thin film increased, the intensity of strain accumulation increased on the ZnO film. Consequently, the grain boundaries changed, leading to changes in the most thermodynamically active sites for ZnO nucleation. Accordingly, ZnO growth was promoted at the grain boundary sites of the ZnO thin film, resulting in the creation of ZnO NWs in a [01–10] diffraction direction. Consistent with these results, the Zn concentration differed between nanostructures (24.3 wt.% for NPs; 31.7 wt.% for NWs). The *d*-spacing also differed between nanostructures (0.257 nm for NPs; 0.261 nm for NWs), and the main peak of diffraction plane shifted from 34.6° (NPs) to 34.4° (NWs). Antibacterial properties of films are related to their thickness and deposition conditions (Cao et al. 2010). Optimization of deposition conditions was necessary; excessive thickness or high bonding conditions decrease Zn release owing to strong attachment of Zn ions to the STS316L substrates. A ZnO NW film with optimal thickness, high R_a, a high Zn concentration on the surface, high H_V and K_{IC} was produced by RF magnetron sputtering. This structure was suitable for use as an antimicrobial agent with high durability.

The antimicrobial pathways of Zn ions depend on active oxygen (Imlay 2013). Zn ions combine with bacterial proteins in the cell and cell wall. They can destroy the DNA and membranes of cells via protein interactions. Therefore, the antimicrobial effect increased as the Zn ion contact areas increased (i.e., from NP to NW structures) because the enhancement in the Zn concentration increased the surface roughness of the ZnO film, increasing the contact surface between microbes and Zn ions. In all specimens (STS316L, ZnO NP, and NW), the number of *E. coli* colonies was slightly lower than that of *S. aureus* colonies. Generally, *S. aureus* cells (gram-positive bacteria) have a thicker peptidoglycan layer than that of *E. coli* cells (gram-negative bacteria). This difference can explain the higher viability of *S. aureus* grown on substrates. The *P. funiculosum* (fungal cell) strains had a higher viability than those of *E. coli* and *S. aureus* (bacterial cells). This may be explained by the larger size of *P. funiculosum* compared with *E. coli* and *S. aureus* as well as its spores, high proliferation, and high antigenicity; these properties make it difficult to destroy *P. funiculosum* cells (Jain et al. 2013). However, we confirmed that ZnO NW structures had high antimicrobial activity, i.e., greater than 99.9% inhibition of *E. coli*, *S. aureus*, and *P. funiculosum*.

To confirm the safety of ZnO NW films with excellent antimicrobial activity, skin irritation and elution behavior were evaluated. When the ZnO NW film contacts various microbes, the bacterial cell walls can be destroyed via the cation effect (Imlay 2013), as shown in Figs. 3 and 4. The amount of eluted Zn ions is determined by the diffusion process, and is directly proportional to the concentration of Zn on the surface and the contact area between microbes and ZnO films. Therefore, a balance between antimicrobial activity and elution concentration was necessary. According to the test results, the ZnO NW film on the stainless steel substrate was a non-irritant. The concentration of eluted Zn ions was approximately 27.2 ± 3.0 μg L^{-1} from the ZnO NW film, which was within the WHO guidelines. Based on these results, we conclude that the antimicrobial ZnO NW structures were non-irritating and satisfied the WHO guidelines for drinking water.

In summary, nanostructured ZnO films with different roughness, wettability, and concentrations were fabricated on stainless steel substrates by RF magnetron sputtering. We confirmed that the patterned ZnO NW structures enabled increased microbe attachment and proliferation owing to their high surface energy, Zn concentration, surface roughness, and wettability. As a result, the ZnO NW film on stainless steel exhibited over 99.9% antibacterial activity. The skin irritation tests demonstrated that the ZnO NW is a non-irritant material. The amount of Zn ions eluted from the ZnO NW film satisfies the WHO guidelines for drinking water. The H_V and K_{IC} values of the ZnO NW were higher than those of the parent stainless steel by approximately 11 and 14%, respectively. These properties of nanostructured ZnO films suggest that ZnO NW structures have valuable applications in various fields, including water pipes, faucets, and stainless steel containers.

Acknowledgements This research was supported by the Basic Research Laboratory Program (Grant ID: NRF-2015041523) through the National Research Foundation of Korea (NRF) funded by the Ministry of Science, ICT & Future Planning. The authors would like to thank Dr. D. Oh from the Korea Testing and Research Institute for performing the skin irritation tests. We also thank Dr. G. Shim for his critical reading of the manuscript and for assistance with the data analysis.

Compliance with ethical standards All animal experiments were carried out with the approval (nr 2015–82) of the Korea Testing and Research Institute. All applicable international, national, and institutional guidelines for the care and use of animals were followed.

Conflict of interest The authors declare that they have no conflict interest.

References

Acocella MR, Corcione CE, Giuri A, Maggio M, Maffezzoli A, Guerra G (2016) Graphene oxide as a catalyst for ring opening reactions in amine crosslinking of epoxy resins. RSC Adv 6(28):23858–23865. doi:10.1039/C6RA00485G

Ashworth DJ, Alloway BJ (2004) Soil mobility of sewage sludge-derived dissolved organic matter, copper, nickel and zinc. Environ Pollut 127(1):137–144. doi:10.1016/S0269-7491(03)00237-9

Biroju RK, Giri PK, Dhara S, Imakita K, Fujii M (2013) Graphene-assisted controlled growth of highly aligned ZnO nanorods and nanoribbons: growth mechanism and photoluminescence properties. ACS Appl Mater Interfaces 6(1):377–387. doi:10.1021/am404411c

Boveris A, Musacco-Sebio R, Ferrarotti N, Saporito-Magriñá C, Torti H, Massot F, Repetto MG (2012) The acute toxicity of iron and copper: biomolecule oxidation and oxidative damage in rat liver. J Inorg Biochem 116:63–69. doi:10.1016/j.jinorgbio.2012.07.004

Byarugaba DK (2004) A view on antimicrobial resistance in developing countries and responsible risk factors. Int J Antimicrob Agents 24: 105–110. doi:10.1016/j.ijantimicag.2004.02.015

Cao XL, Cheng C, Ma YL, Zhao CS (2010) Preparation of silver nanoparticles with antimicrobial activities and the researches of their biocompatibilities. J Mater Sci Mater Med 21:2861–2868. doi:10.1007/s10856-010-4133-2

Choi HJ, Park BJ, Eom JH, Choi MJ, Yoon SG (2015) Achieving antifingerprinting and antibacterial effects in smart-phone panel applications using ZnO thin films without a protective layer. ACS Appl Mater Interfaces 8:997–1003. doi:10.1021/acsami.5b11024

Dietrich AM, Burlingame GA (2015) Critical review and rethinking of USEPA secondary standards for maintaining organoleptic quality of drinking water. Environ Sci Technol 49(2):708–720. doi:10.1021/es504403t

Djemai-Zoghlache Y, Isambert A, Belhaneche-Bensemra N (2011) Electrochemical behavior of the 316L steel type in a marine culture of microalgae (*Porphyridium purpureum*) under the 12/12 h photoperiod and effect of different working electrode exposure conditions on the biofilm–metal interface. J Ind Microbiol Biotechnol 38: 1969–1978. doi:10.1007/s10295-011-0986-8

Djeribi R, Bouchloukh W, Jouenne T, Menaa B (2012) Characterization of bacterial biofilms formed on urinary catheters. Am J Infect Control 40:854–859. doi:10.1016/j.ajic.2011.10.009

Drake PL, Hazelwood KJ (2005) Exposure-related health effects of silver and silver compounds: a review. Ann Occup Hyg 49:575–585. doi:10.1093/annhyg/mei019

Gholap H, Warule S, Sangshetti J, Kulkarni G, Banpurkar A, Satpute S, Patil R (2016) Hierarchical nanostructures of Au@ ZnO: antibacterial and antibiofilm agent. Appl Microbiol Biot 100(13):5849–5858. doi:10.1007/s00253-016-7391-1

He L, Liu Y, Mustapha A, Lin M (2011) Antifungal activity of zinc oxide nanoparticles against *Botrytis cinerea* and *Penicillium expansum*. Microbiol Res 166:207–215. doi:10.1016/j.micres.2010.03.003

Imlay JA (2013) The molecular mechanisms and physiological consequences of oxidative stress: lessons from a model bacterium. Nat Rev Microbiol 11(7):443–454. doi:10.1038/nrmicro3032

Jain N, Bhargava A, Tarafdar JC, Singh SK, Panwar J (2013) A biomimetic approach towards synthesis of zinc oxide nanoparticles. Appl Microbiol Biot 97(2):859–869. doi:10.1007/s00253-012-3934-2

Josephs-Spaulding J, Beeler E, Singh OV (2016) Human microbiome versus food-borne pathogens: friend or foe. Appl Microbiol Biot 100(11):4845–4863. doi:10.1007/s00253-016-7523-7

Kuang H, Yang L, Shah NP, Aguilar ZP, Wang L, Xu H, Wei H (2016) Synergistic in vitro and in vivo antimicrobial effect of a mixture of ZnO nanoparticles and Lactobacillus fermentation liquor. Appl Microbiol Biot 100(8):3757–3766. doi:10.1007/s00253-015-7221-x

Kumar R, Münstedt H (2005) Silver ion release from antimicrobial polyamide/silver composites. Biomaterials 26:2081–2088. doi:10.1016/j.biomaterials.2004.05.030

Kumar M, Tekcan B, Okyay AK (2014) Atomic layer deposited HfO_2 based metal insulator semiconductor GaN ultraviolet photodetectors. Curr Appl Phys 14:1703–1706. doi:10.1016/j.cap.2014.10.001

Madhumitha G, Elango G, Roopan SM (2016) Biotechnological aspects of ZnO nanoparticles: overview on synthesis and its applications. Appl Microbiol Biot 100(2):571–581. doi:10.1007/s00253-015-7108-x

Makris KC, Andra SS, Botsaris G (2014) Pipe scales and biofilms in drinking-water distribution systems: undermining finished water quality. Crit Rev Environ Sci Technol 44(13):1477–1523. doi:10.1080/10643389.2013.790746

Martin JGP, e Silva GDO, da Fonseca CR, Morales CB, Silva CSP, Miquelluti DL, Porto E (2016) Efficiency of a cleaning protocol for the removal of enterotoxigenic *Staphylococcus aureus* strains in dairy plants. Int J Food Microbiol 238:295–301. doi:10.1016/j.ijfoodmicro.2016.09.018

Mishra N, Rai VK, Yadav KS, Sinha P, Kanaujia A, Chanda D, Yadav NP (2016) Encapsulation of mentha oil in chitosan polymer matrix alleviates skin irritation. AAPS PharmSciTech 17(2):482–492. doi:10.1208/s12249-015-0378-x

Okeke IN, Klugman KP, Bhutta ZA, Duse AG, Jenkins P, O'Brien F, Pablos-Mendez A, Laxminarayan R (2005) Antimicrobial resistance in developing countries. Part II: strategies for containment. Lancet Infect Dis 5:568–580. doi:10.1016/S1473-3099(05)70217-6

Parikh DV, Fink T, Rajasekharan K, Sachinvala ND, Sawhney APS, Calamari TA (2005) Antimicrobial silver/sodium carboxymethyl cotton dressings for burn wounds. Text Res J 75:134–138. doi:10.1177/004051750507500208

Ren G, Hu D, Cheng EW, Vargas-Reus MA, Reip P, Allaker RP (2009) Characterisation of copper oxide nanoparticles for antimicrobial applications. Int J Antimicrob Agents 33:587–590. doi:10.1016/j.ijantimicag.2008.12.004

Rouxel T, Sellappan P, Célarié F, Houizot P, Sangleboeuf JC (2014) Toward glasses with better indentation cracking resistance. CR Mec 342:46–51. doi:10.1016/j.crme.2013.10.008

Saravanakumar B, Kim SJ (2014) Growth of 2D ZnO nanowall for energy harvesting application. J Phys Chem C 118(17):8831–8836. doi:10.1021/jp502057p

Sellappan P, Rouxel T, Célarié F, Becker E, Houizot P, Conradt R (2013) Composition dependence of indentation deformation and indentation cracking in glass. Acta Mater 61:5949–5965. doi:10.1016/j.actamat.2013.06.034

Sin MC, Sun YM, Chang Y (2014) Zwitterionic-based stainless steel with well-defined polysulfobetaine brushes for general bioadhesive control. ACS Appl Mater Interfaces 6(2):861–873. doi:10.1021/am4041256

Tamvakos A, Calestani D, Tamvakos D, Mosca R, Pullini D, Pruna A (2015) Effect of grain-size on the ethanol vapor sensing properties of room-temperature sputtered ZnO thin films. Microchim Acta 182(11–12):1991–1999. doi:10.1007/s00604-015-1539-z

Vasudevan S, Oturan MA (2014) Electrochemistry: as cause and cure in water pollution-an overview. Environ Chem Lett 12(1):97–108. doi:10.1007/s10311-013-0434-2

Zhang C, Li C, Chen Y, Zhang Y (2014) Synthesis and catalysis of Ag nanoparticles trapped into temperature-sensitive and conductive polymers. J Mater Sci 49:6872–6882. doi:10.1007/s10853-014-8389-7

Žvab U, Marušič MB, Štangar UL (2012) Microplate-based assays for the evaluation of antibacterial effects of photocatalytic coatings. Appl Microbiol Biot 96(5):1341–1351. doi:10.1007/s00253-012-4458-5